IPPI

Polyolefins Journal, Vol. 10, No. 3 (2023)
DOI: 10.22063/POJ.2023.3310.1251

ORIGINAL PAPER

Confinement effect of blocks on the morphology of composite particles in the co-assembly of block copolymers/homopolymers

Elmira Khaksar[1,2], Marzieh Golshan[1,2], Hossein Roghani-Mamaqani[1,2], Mehdi Salami-Kalajahi[1,2,*]

[1]Faculty of Polymer Engineering, Sahand University of Technology, P.O. Box 51335-1996, Tabriz, Iran
[2]Institute of Polymeric Materials, Sahand University of Technology, P.O. Box 51335-1996, Tabriz, Iran

Received: 18 February 2023, Accepted: 26 March 2023

ABSTRACT

In this study, reversible addition-fragmentation chain transfer (RAFT) polymerization was used to synthesize hydrophobic polystyrene (PS), poly(methyl acrylate) (PMA), and poly(methyl acrylate-*b*-styrene) (PMA-*b*-PS) block copolymers with three distinct molecular weights. Polyaniline (PANI) was synthesized by electrochemical method. Proton nuclear magnetic resonance (^{1}H NMR) and gel permeation chromatography (GPC) have both been used to examine the properties of the polymers synthesized. In aqueous media at room temperature, PANI has been co-assembled with PS, PMA, and PMA-*b*-PS. The size and morphology of the co-assembled structures have been examined using transmission electron microscopy (TEM), dynamic light scattering (DLS), and field emission scanning electron microscopy (FE-SEM). According to the findings, polymers hydrophobicity increased with increasing molecular weight, causing faster precipitation in aqueous solution and a reduction in particle size. The results demonstrated that adding conductive polymer produced core-shell morphologies, while the core morphologies are different. Thermodynamic principles governed morphology, and the most likely morphology to develop was the one that minimized the total surface free energy. The polymers caused the surface tension between the polymers with water and the surface tension between the primary polymer and the secondary polymer to be reduced by overlapping each other and precipitation. **Polyolefins J (2023) 10: 137-147**

Keywords: Conductive polymer; assembly; core-shell particles; block copolymer.

INTRODUCTION

Block copolymers are polymers that are formed by polymerization of two or more different monomers that polymer can be made with different structures. The unique feature of block copolymers is their ability to form nanoscale structures [1-3]. In this regard, by changing various parameters including, polymerization degree, volume fraction, and Flory-Huggins interaction parameter, different morphologies such as Janus, micellar, and snowman are obtained [4-6]. Attractive properties of self-assembling polymers and copolymers in fields of morphology [7], water purification [8], and dye absorption [9] have received much attention. The morphology that results from block copolymer self-assembly is related to two driving forces: repulsion caused by incompatibility with the environment and chemical bonding which limits phase separation leading

---

[*] Corresponding Author - E-mail: m.salami@sut.ac.ir

to microphase rather than macrophase [10]. In the meantime, electroactive polymers are sensitive due to their high electrical conductivity to electrical stimuli and respond by changing their size and shape. Polyaniline (PANI) [11], polythiophene [12], polypyrrole (PPy) [13], and polyacetylene [14] are the most often utilized conductive polymers. PANI has more stability than other conductive polymers. Therefore, it has been studied and used in a variety of fields including activators [15], batteries [16], solar cells [17], artificial muscles [18], and drug delivery systems [19]. For the creation of hybrid materials, co-assembly of block copolymers with inorganic nanoparticles in solution has garnered great attention. The fundamentals of self-assembling blocks copolymers can be utilized to change the morphology of a co-assembly. However, it is currently difficult to predict how nanoparticles would affect the self-assembly of block copolymers. The presence of nanoparticles may further complicate the size and structure of co-assembly [20-22]. Copolymer self-assembly has resulted in a number of different shapes, including spherical micelles [23], rods [24], bicycles [25], and Janus nanoparticles [26], among others. In this study, PMA-*b*-PS was synthesized by reversible addition-fragmentation chain transfer (RAFT) polymerization in a variety of molecular weights. PANI has also been created through electrochemical polymerization. Copolymers of PMA-*b*-PS and PANI have been co-assembled in aqueous media at room temperature. Also, co-assembly of PANI with PS and PMMA has been studied to investigate the confinement effect of chemical bonding on co-assembly process. Different thermodynamical methods and analysis have been used to study the morphology of the produced composite particles.

EXPERIMENTAL

Synthesis of polyaniline (PANI)

Aniline (16.6 mg/mL) was mixed with ammonium persulfate (0.05 mg/mL in 20 mL H_2O), and the reaction was then carried out at 30°C for 6 h. The filtered liquid was then repeatedly rinsed with distilled water and methanol. Finally, PANI was dried for 48 h at 70°C in a vacuum oven. 60% gravimetrically was used to calculate the reaction yield [11].

Synthesis PMA as macroRAFT agent

PMAs with different molecular weights were synthesized via RAFT polymerization. The molar ratio of AIBN as initiator and cyanomethyl dodecyl trithiocarbonate (CMDTTC, Supporting Information) as RAFT agent was 1:5 and THF was used as a solvent in volumetric proportion to the monomer. For synthesis of PMA homopolymers, three different [monomer]/[RAFT] ratios of 100, 300, and 500 were used. After adding monomer, RAFT agent, and solvent into a glass vial under nitrogen atmosphere, initiator was added and temperature was increased to 65°C. After 6 h, sample was precipitated in methanol and after three times of purification, polymer was dried in a vacuum oven at 60°C overnight. Finally, degree of polymerization for each sample was measured by ^{1}H NMR, and samples were named as PMA75, PMA256, and PMA455. Moreover, polystyrene homopolymers were synthesized for comparative study using the same procedure and named PS100, PS292, and PS480, respectively.

Synthesis of block copolymers

Using CMDTTC as the RAFT agent, PMA-*b*-PS block copolymers were synthesized [27]. The molar ratio of the macroRAFT agent:AIBN was 5:1, and the solvent, THF, was utilized in volumetric proportion to the monomer. For synthesis of PMA-*b*-PS block copolymers, the [monomer]/[macroRAFT agent] ratio of 100 for PMA75, 300 for PMA256, and 500 for PMA455 was used. Initiator was added, temperature was raised to 65°C, and the glass vial was then filled with monomer, macroRAFT agent, and solvent. After 24 h, the sample was precipitated in methanol, and the copolymer was then purified three times before being dried in a vacuum oven at 60°C for 24h. Ultimately, ^{1}H NMR was used to determine the degree of polymerization for each sample, and the samples were given the names PMA75-*b*-PS85, PMA256-*b*-PS210, and PMA455-*b*-PS301.

Co-assembly of PMA-*b*-PS and PANI

For co-assembly studies, DMF (2 mg mL^{-1}) was used to dissolve PMA-*b*-PS and PANI in a weight ratio of

1:1. The solution was then diluted with distilled water at room temperature (one drop every 10 seconds), resulting in a concentration of PMA-*b*-PS@PANI of 0.2 mg mL^{-1}. Solutions were then agitated for a further 40 minutes at 25°C [28]. PS, PMA, and PANI (weight ratio of 1:1:2) were co-assembled taking into account various molecular weights of the homopolymers in order to evaluate the impact of copolymerization on the morphology of self-assembled structures.

RESULTS AND DISCUSSION

Characteristics of copolymers

PMA-*b*-PS block copolymers with different molecular weights were created using RAFT polymerization. The molecular weight of each sample and other molecular characteristics were ascertained using ^{1}H NMR and GPC, and the results are shown in Figures 1 to 3. According to ^{1}H NMR spectra for homopolymers and block copolymers, the signals of methylene protons next to the sulfur atoms were detected at 2.17-2.50 ppm [29], the signals related to methine and methylene protons in the backbone of PS were detected at 1.00-2.15 ppm, and the signals related to methine protons in the backbone of PMA were detected at 2.15-2.45 ppm for [monomer]:[RAFT] ratios of 100, 300, and 500, respectively, and the degrees of polymerization of PMA were predicted to be 75, 256, and 455 correspondingly. Eventually, for [monomer]:[RAFT] ratios of 100, 300, and 500, respectively, the degree of PS polymerization in PMA-*b*-PS was estimated to be 85, 210, and 301. The molecular weights obtained by GPC (Figure 3) were consistent with those ascertained from ^{1}H NMR spectra, as reported in Table 1. There was low dispersion (Đ) and homogeneous molecular weight distribution in all samples.

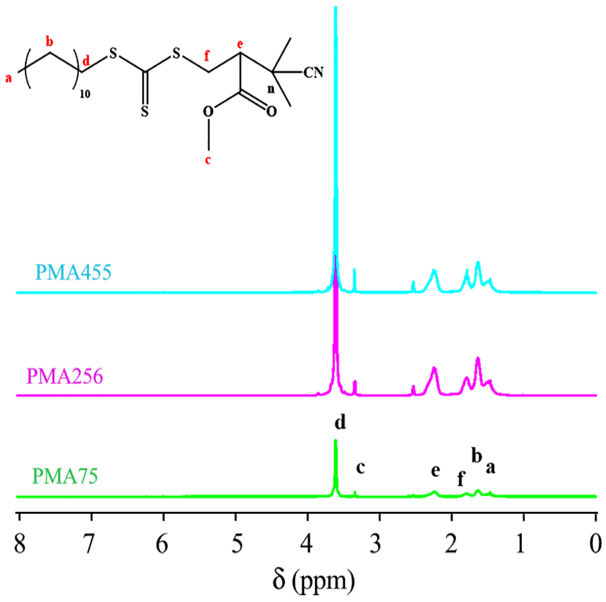

Figure 1. ^{1}H NMR spectra of PMA75, PMA256, and PMA455.

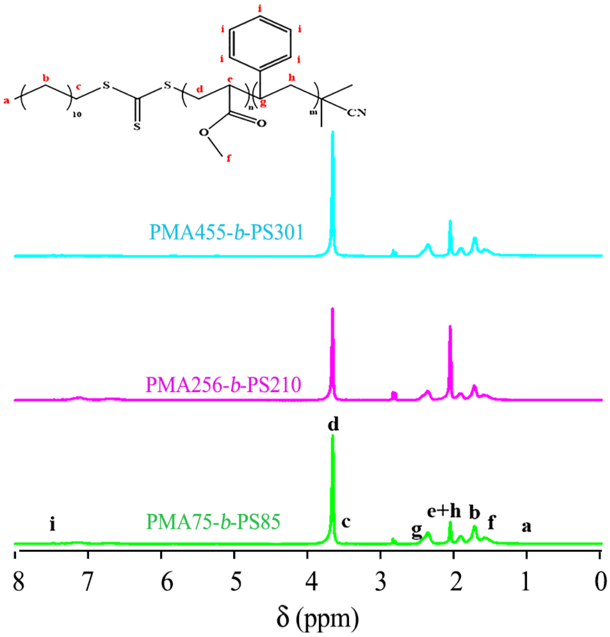

Figure 2. ^{1}H NMR spectra of block copolymers.

Co-assembly behavior of block copolymers in the presence of PANI

A regular morphology is created by the co-assembly

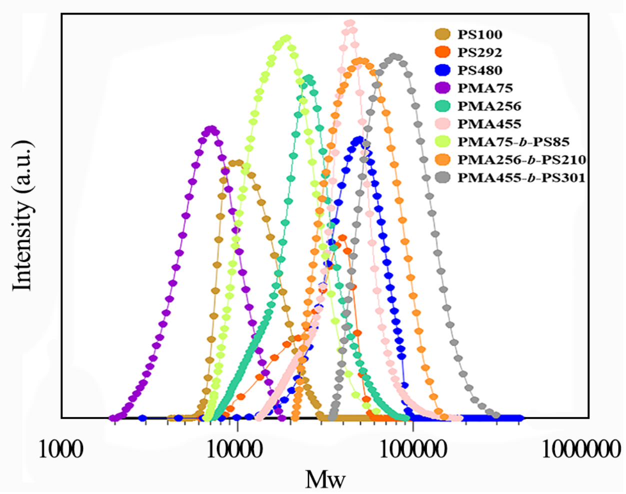

Figure 3. GPC profiles of PS, PMA, and PMA-*b*-PS block copolymers.

Table 1. $M_{n,th}$, M_n (^{1}H NMR, g/mol), and M_n (GPC, g/mol) of synthesized polymers.

Polymers	$M_{n,th}$$^{(a)}$ (g/mol)	M_n (^{1}H NMR, g/mol)	M_n (GPC, g/mol)	Đ (GPC)
PMA75	8955	6802	6200	1.15
PMA256	26173	22401	21090	1.19
PMA455	43391	39571	36510	1.14
PS100	10761	12114	10710	1.14
PS292	31591	30799	29500	1.15
PS480	52421	50353	47840	1.11
PMA75-*b*-PS85	19369	15655	14900	1.18
PMA256-*b*-PS210	57417	44334	43160	1.21
PMA455-*b*-PS301	95465	70986	69620	1.19

$^{(a)}$ $$M_{n,\text{th}} = MW_{RAFT} + \frac{[M]_0 MW_{Monomer} \cdot p}{[\text{RAFT}]_0 + 2[AIBN]}$$

behavior of polymers in solution and is dependent on interactions between the polymer, solvent, and concentration. According to Figures 4-6, the results demonstrated that diverse morphologies may be produced by varying the polymer's molecular weight. FE-SEM was used to examine the morphology of co-assembled polymers while PANI was present.

Table 2 demonstrates how to determine the polydispersity index (*PDI*), weight-average diameter (D_w), and number-average diameter (D_n) of co-assembled structures using Equations (1) through (3) [31,32].

$$D_n = \frac{\sum_{i=1}^{n} n_i D_i}{\sum_{i=1}^{n} n_i} \qquad (1)$$

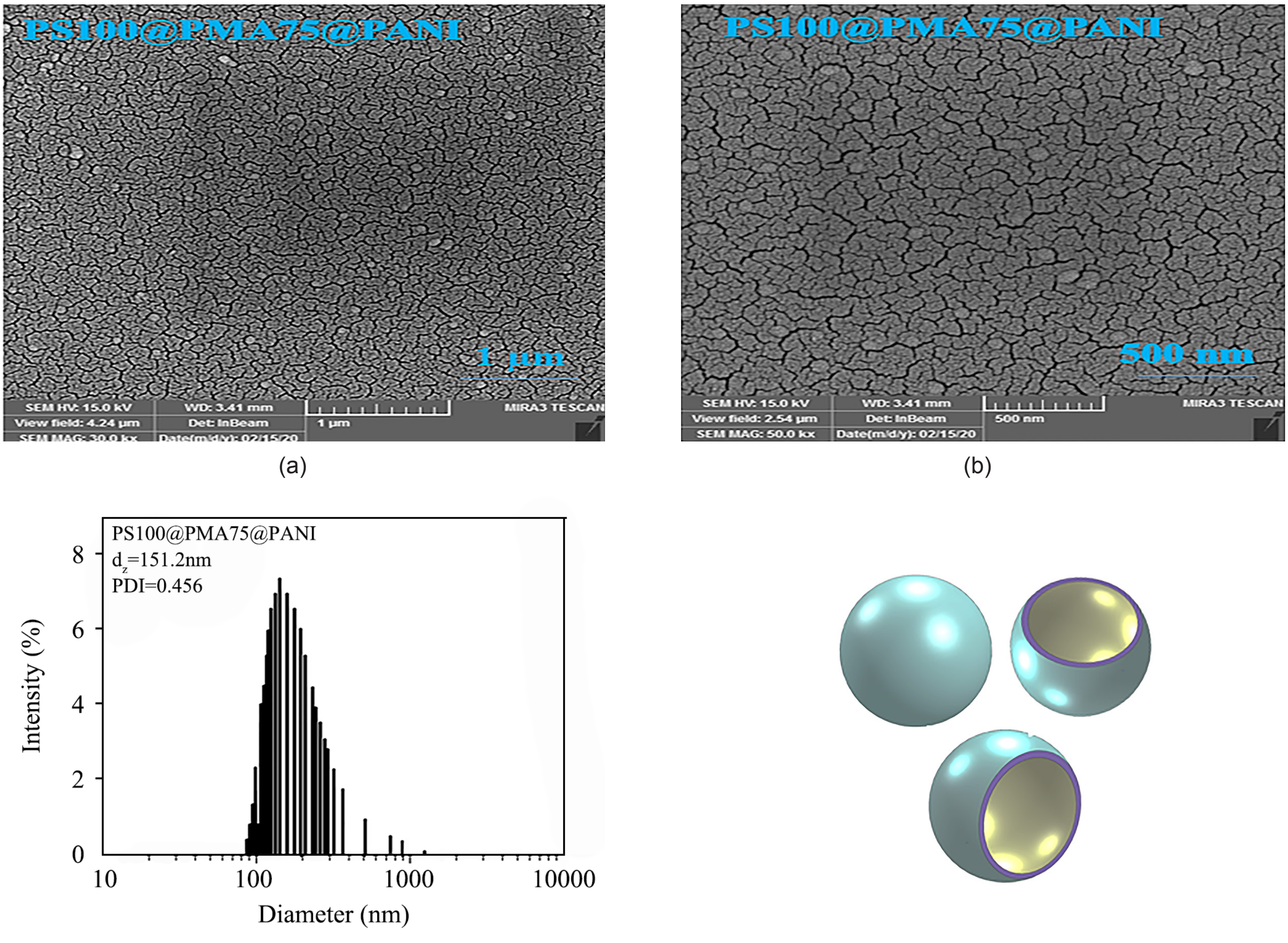

(a) (b)

(c) (d)

Figure 4. FE-SEM image (a, b), DLS result (c), and schematic morphology (d) of PS100@PMA75@PANI.

$$D_W = \frac{\sum_{i=1}^{n} n_i D_i^4}{\sum_{i=1}^{n} n_i D_i^3} \qquad (2)$$

$$PDI = \frac{D_W}{D_n} \qquad (3)$$

Co-assembly has been carried out at a concentration of 0.2 mg/mL in each sample. As a result, the system has low viscosity, and thermodynamic parameters should frequently regulate the morphology of composite particles [33]. The most probable existing morphology is the one that thermodynamically minimizes the total interfacial free energy (GS) [34]. Equation (4) gives the changes in total free energy (G) [35,36].

$$\sum \sigma_{ij} A_{ij} - \sigma_0 A_0 = G_S - \sigma_0 A_0 \qquad (4)$$

Parameters in Equation (4) are defined as follows: total interfacial free energy (G_S), the interfacial tension between phases i and j (σ_{ij}), the corresponding interfacial area (A_{ij}), the interfacial tension (σ_0), and the interfacial area (A_0). Primary polymer/water, secondary polymer/water, and primary polymer/secondary polymer are the three interfaces present in these systems. As a result, morphology is established by the creation of the smallest free energy-minimizing interface between two polymers. The free energy of the total particle surface is minimized by producing the lowest interface between two polymer components and each polymer with water. In this respect, contact angle data can be used to calculate the surface energy of samples using the Owens-Wendt Equation [37,38] (Figure S3).

$$\gamma_L (1 + COS\theta) = 2\sqrt{\gamma_s^d \gamma_l^d} + 2\sqrt{\gamma_s^p \gamma_l^p} \qquad (5)$$

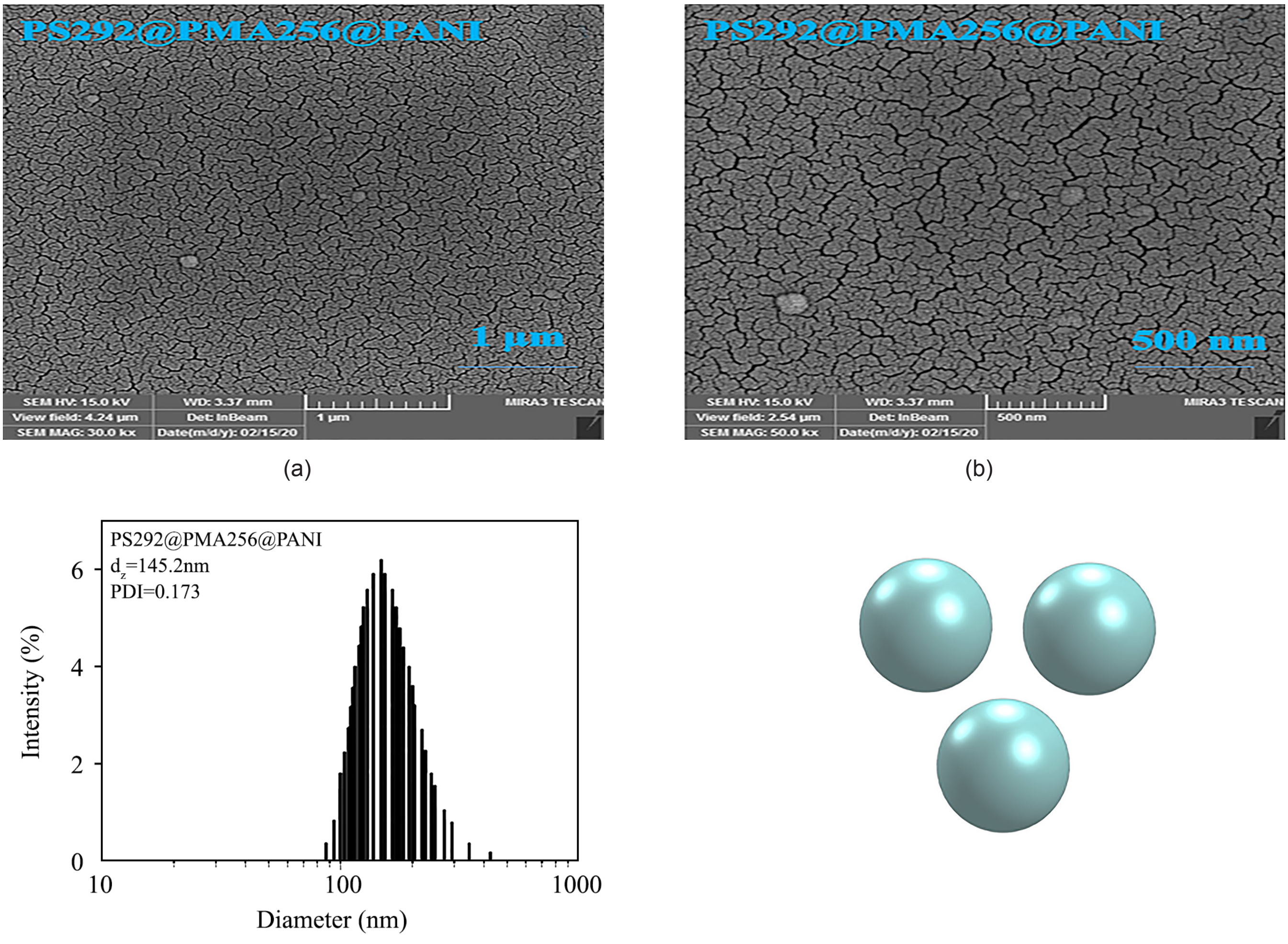

(a) (b) (c) (d)

Figure 5. FE-SEM image (a, b), DLS result (c), and schematic morphology (d) of PS292@PMA256@PANI.

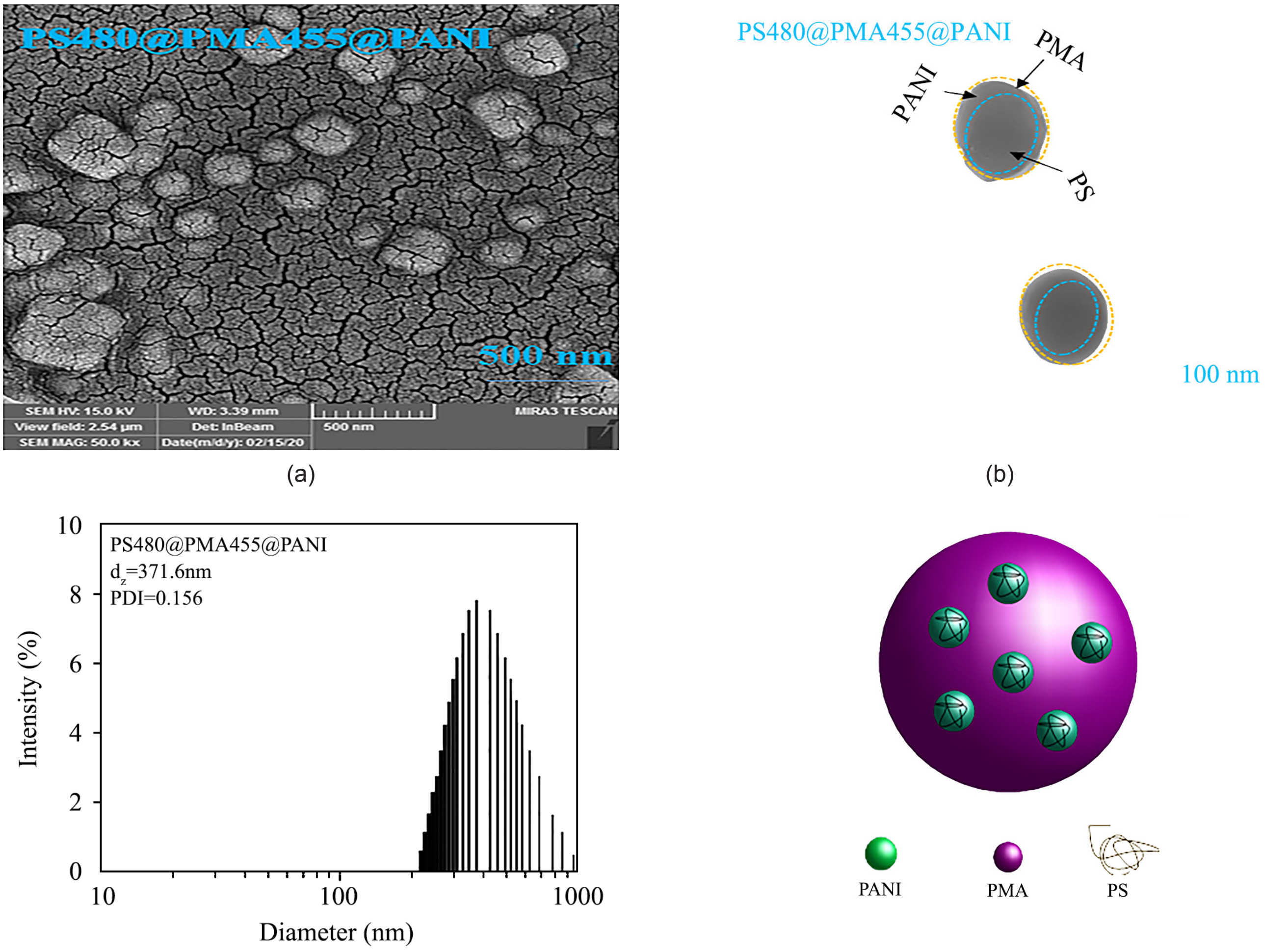

(a) (b)

(c) (d)

Figure 6. FE-SEM image (a), TEM image (b), DLS result (c), and schematic morphology (d) of PS480@PMA455@PANI.

Parameters in Equation (5) are defined as follows: the contact angle (θ), liquid surface tension (γ_L), solid surface free energy (γ_S), dispersive components (d), and polar components (p). It is necessary to measure the contact angles with a polar fluid (distilled water) and a non-polar fluid (diiodomethane) in order to identify the dispersive and polar components of surface free energy. Table 3 displays the dispersive and polar components of the surface tension of the test fluids at room temperature. Equations (6) and (7) can be used to determine the surface stress of each phase as well as the surface stress between two phases [39].

$$\gamma_i = \gamma_i^d + \gamma_i^p \qquad (6)$$

$$\gamma_{12} = \gamma_1 + \gamma_2 - \frac{4\gamma_1^d \gamma_2^d}{\gamma_1^d + \gamma_2^d} - \frac{4\gamma_1^p \gamma_2^p}{\gamma_1^p + \gamma_2^p} \qquad (7)$$

The results of Equations (6) and (7) are presented in The results of FE-SEM, TEM, and DLS for co-assembled homopolymers PS@PMA@PANI are displayed in Figures 4 to 6. PS with three different degrees of polymerizations (100, 292, and 480) and PMA with three different degrees of polymerizations (75, 255, and 455) were co-assembled in the presence of PANI conductive polymer. Table S6 shows that the stresses

Table 2. Weight-average diameter, number-average diameter, and polydispersity index of self-assembled structures.

Sample	D_n (nm)	D_w (nm)	*PDI*	Sample	D_n (nm)	D_w (nm)	*PDI*
PS100@PMA75@PANI	71.9	74.1	1.03	**PMA75-*b*-PS85@PANI**	244.3	242.6	1.04
PS292@PMA256@PANI	102.3	119.8	1.17	**PMA75-*b*-PS85@PANI**	97.8	156.0	1.08
PS480@PMA455@PANI	196.3	232.0	1.18	**PMA455-*b*-PS301@PANI**	125.0	131.4	1.05

Table 3. Contact angles of test liquids on polymers.

Sample	Distilled water	Diiodomethane	γ_s^d	γ_s^p	γ_s
PANI	66.8	27.5	45.2	7.3	52.5
PS	99.7	37.6	40.8	0.004	40.8
PMA	72.5	47.9	35.4	7.5	42.9

Table 4. Surface stress measurements and spreading coefficients (mN/m).

Sample	PS	PMA
γ_{12}	56.8	35.6
γ_{13}	7.5	1.2
γ_{23}	40.9	40.9
$\gamma_{PS,PMA}$	7.85	

between PS and water, the stresses between PMA and water, and the stresses between PANI and water are 56.7, 35.6, 40.9, respectively. The results showed that PS and PANI polymers are more hydrophobic than PMAs. PANI coats the surface of PS to reduce stress because PS is more hydrophobic and encounters significant levels of stress with water. Because PANI is more hydrophobic than PMA, PMA acts as the shell of a large core. The core contains PS micelles covered by PANI.

The results of co-assembled PMA75-*b*-PS85@PANI, PMA256-*b*-PS210@PANI, and PMA455-*b*-PS301@PANI are shown in Figures 7-9 for FE-SEM, TEM, and DLS, respectively. In PMA-*b*-PS block copolymers, PMA and PS are bonded together by covalent bonding. By adding nonsolvent, PS and PMA blocks cannot precipitate separately according to the Lattice model in block copolymers. This limit reduces the spatial deformation states, resulting in reducing the amount of irregularity and entropy. PMA-*b*-PS block copolymer and PANI have high surface tension with water and tend to reduce their surface stress to reach a more stable state. Because homopolymer has a higher

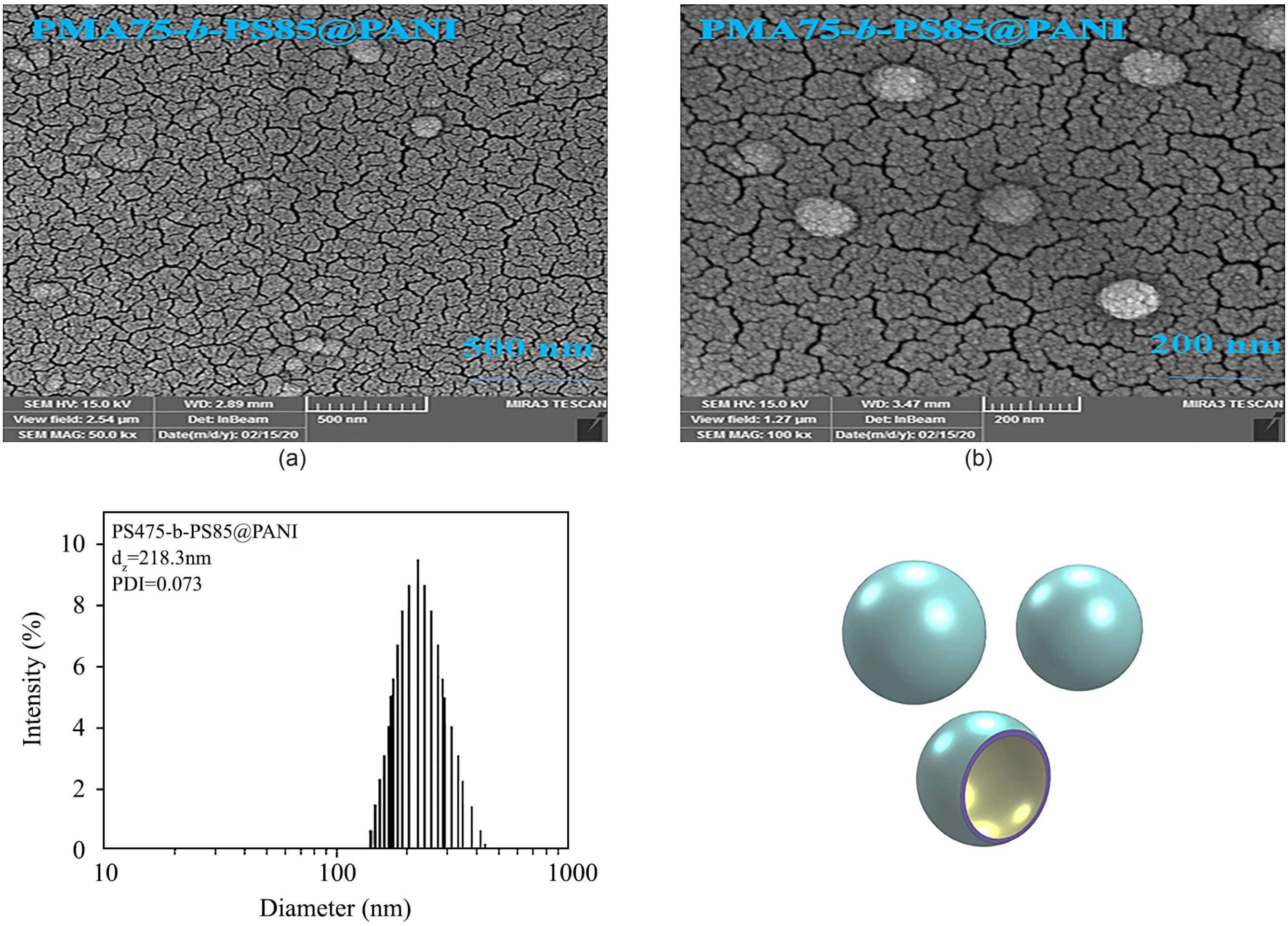

(a) (b)

(c) (d)

Figure 7. FE-SEM image (a, b), DLS result (c), and schematic morphology (d) of PMA75-*b*-PS85@PANI.

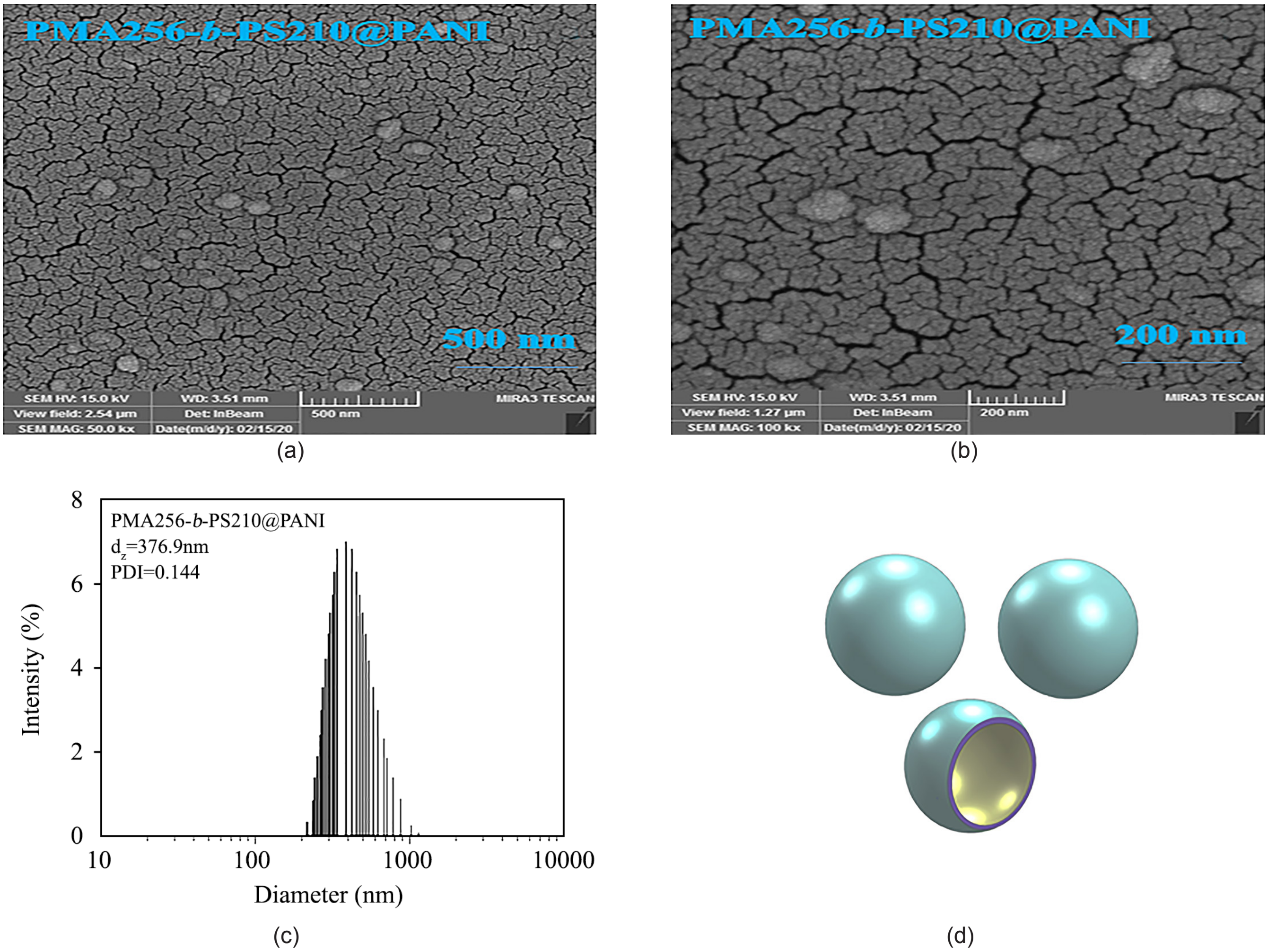

(a) (b) (c) (d)

Figure 8. FE-SEM image (a, b), DLS result (c), and schematic morphology (d) of PMA256-*b*-PS210@PANI.

degree of freedom than block copolymer, PANI seeks to precipitate on a surface that reduces its stress with the environment due to hydrophobicity. Therefore, it moves towards PMA-*b*-PS component and because of π-π interactions, PANI shows a high affinity to PS. Then, it precipitates preferentially on the surface of PS, resulting in reducing the amount of PS stress with water. Additionally, PMA coats the surface of PANI to lessen the water stress on PANI because it is less hydrophobic than PANI. The overall tension of the polymers with water decreased and the free energy lowered with the creation of the core-shell morphology. As the molecular weight increases, the hydrophobicity of the chains increases [40]. As a result, the tendency to precipitation increases, and with earlier deposition, a core is formed. The other polymers, which enlarge the particle size, are positioned near to the core. The particle size of block copolymers is larger than that of homopolymers because in block copolymers the two polymers are connected by a covalent bond. When deposited according to the Lattice model, they have limited movement and thus occupy more space.

CONCLUSIONS

RAFT polymerization was successfully used to create PMA-*b*-PS, PMA, and PMA with three distinct molecular weights, and an electrochemical process was used to create PANI. The behavior of PANI and PMA-*b*-PS copolymers during co-assembly was investigated. Hydrophobic polymers PS, PMA, and PMA-*b*-PS showed a lower contact surface with the solvent as a result of their incompatibility with it, which decreased entropy and produced new core. Additionally, the hydrophobic cores of the co-assembly solutions formed

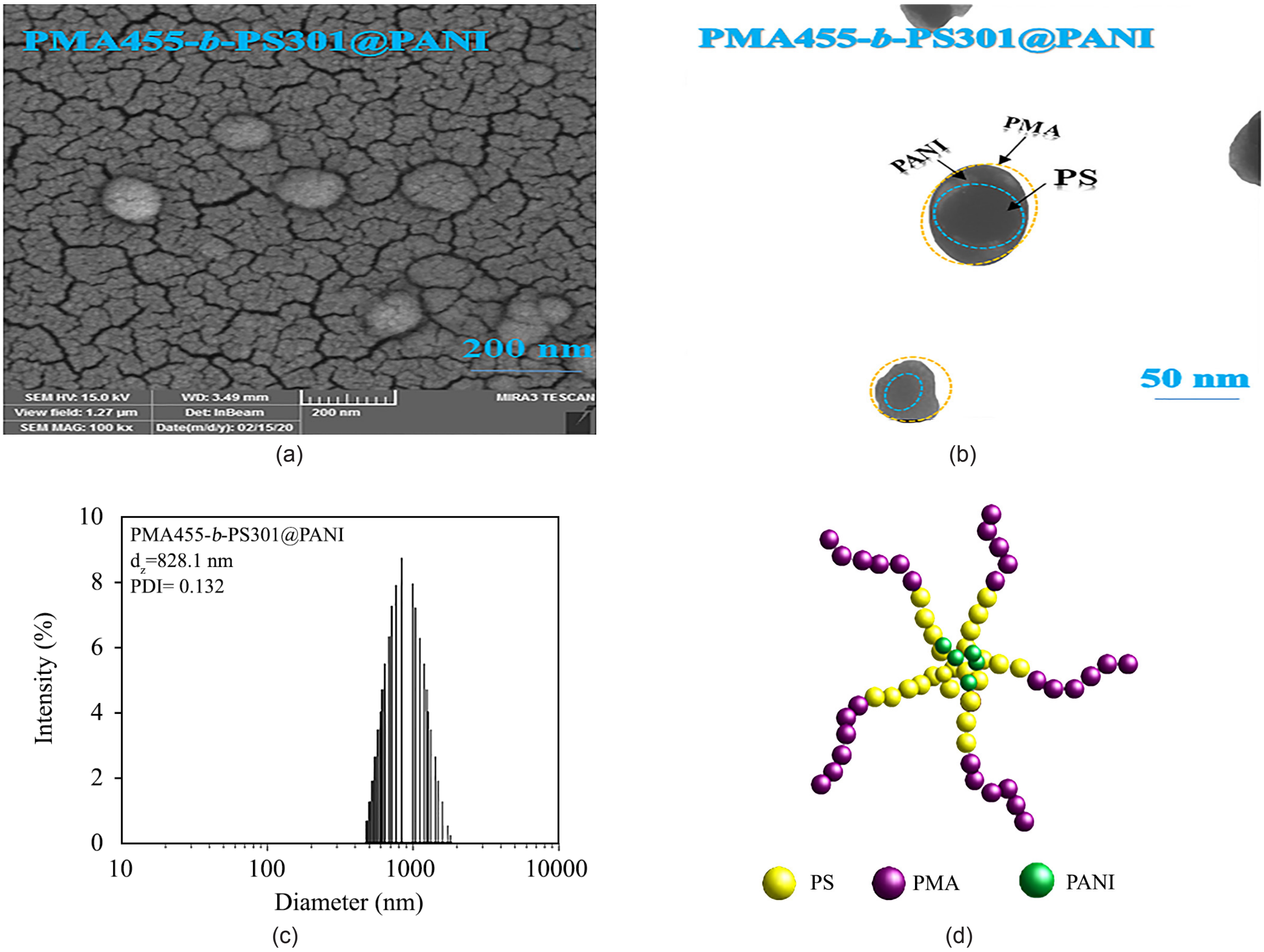

Figure 9. FE-SEM image (a), TEM image (b), DLS result (c), and schematic morphology (d) of PMA455-*b*-PS301@PANI.

a shell due to the presence of conductive polymers in the co-assembly solutions. Thermodynamic principles governed the morphology, and the most likely morphology to develop was the one that minimized the total surface free energy. The polymers caused the surface tension between the polymers with water and the surface tension between the primary polymer and the secondary polymer to be reduced by overlapping each other and precipitation. Due to the thermodynamic relationships, the total free surface stress was minimized by reducing the free energy stress. Co-assembly of two hydrophobic polymers in the presence of conductive polymer (PMA@PS@PANI) showed that homopolymers had no bond with each other so they could move easily and be placed in a place with less stress. Then, a core-shell morphology was formed, the core of which contained spherical core-shell micelles. The results showed that co-assembly of copolymers (PMA-*b*-PS@PANI) in the presence of conductive polymer in solution led to the formation of core-shell morphology.

Supporting information: Materials; Instrumentation; Synthesis of cyanomethyl dodecyl trithiocarbonate (CMDTTC); Contact angle results.

CONFLICT OF INTEREST

The authors declare that they have no conflict of interest.

REFERENCES

1. Mandal P, Patra D, Shunmugam R (2020) Hier-

archical self-assembled nanostructures of lactone-derived thiobarbiturate homopolymers for stimuli-responsive delivery applications. Polym Chem 11: 3340-3348

2. Tanford C (1974) Thermodynamics of micelle formation: prediction of micelle size and size distribution. Proc Natl Acad Sci 71: 1811-1815
3. Muslim A, Zhao Z, Shi Y, Malik D (2017) Secondary self-assembly behaviors of PEO-*b*-PtBA-b-PS triblock terpolymers in solution. Chem Pap 71: 1721-1729
4. Simões FR, Pocrifka LA, Marchesi LFQP, Pereira EC (2011) Investigation of electrochemical degradation process in polyaniline/polystyrene sulfonated self-assembly films by impedance spectroscopy. J Phys Chem B 115: 11092-11097
5. Amani F, Dehghani E, Salami-Kalajahi M (2021) Preparation and study on properties of dual responsive block copolymer-grafted polypyrrole smart Janus nanoparticles. J Polym Res 28: 142
6. Blasco E, Schmidt BV, Barner-Kowollik C, Piñol M, Oriol L (2013) Dual thermo- and photo-responsive micelles based on miktoarm star polymers. Polym Chem 4: 4506-4514
7. Farbod F, Goharpey F, Salami-Kalajahi M, Khonakdar HA (2022) Synthesis and self-assembly of polystyrene block polyacrylic acid for sub 10 nm feature size. React Funct Polym 178: 105352
8. Feng X, Imran Q, Zhang YL, Sixdenier X, Lu X, Kaufman G, Osuji CO (2019) Precise nanofiltration in a fouling-resistant self-assembled membrane with water-continuous transport pathways. Sci Adv 5: eaav9308
9. Cheng CC, Chiu TW, Yang XJ, Huang SY, Fan W, Lai JY, Lee DJ (2019) Self-assembling supramolecular polymer membranes for highly effective filtration of water-soluble fluorescent dyes. Polym Chem 10: 827-834
10. Liu W, Mao J, Xue Y, Zhao Z, Zhang H, Ji X (2016) Nanoparticle loading induced morphological transitions and size fractionation of coassemblies from PS-*b*-PAA with quantum dots. Langmuir 32: 7596-7605
11. Feng X, Yang G, Xu Q, Hou W, Zhu JJ (2006) Self-assembly of polyaniline/Au composites: From nanotubes to nanofibers. Macromol Rapid Commun 27: 31-36
12. Kumar D, Sharma RC (1998) Advances in conductive polymers. Eur Polym J 34: 1053-1060
13. Khadem F, Pishvaei M, Salami-Kalajahi M, Najafi F (2017) Morphology control of conducting polypyrrole nanostructures via operational conditions in the emulsion polymerization. J Appl Polym Sci 134: 44697
14. Shirakawa H, Ikeda S (1971) Infrared spectra of poly(acetylene). Polym J 2: 231-244
15. Lahav M, Durkan C, Gabai R, Katz E, Willner I, Welland ME (2001) Redox activation of a polyaniline-coated cantilever: An electro-driven microdevice. Angew Chem 113: 4219-4221
16. Nakajima T, Kawagoe T (1989) Polyaniline: Structural analysis and application for battery. Synth Met 28: 629-638
17. Li Q, Wu J, Tang Q, Lan Z, Li P, Lin J, Fan L (2008) Application of microporous polyaniline counter electrode for dye-sensitized solar cells. Electrochem Commun 10: 1299-1302
18. Beregoi M, Evanghelidis A, Matei E, Enculescu I (2017) Polyaniline based microtubes as building-blocks for artificial muscle applications. Sens Actuator B-Chem 253: 576-583
19. Lei Y, Zhou J, Yao Z, Li L (2020) Self-assembly of porous polyaniline microspheres via template-free interfacial method for high-performance electromagnetic absorption property. Mater Lett 265: 127389
20. Mai Y, Eisenberg A (2012) Self-assembly of block copolymers. Chem Soc Rev 41: 5969-5985
21. Liu W, Mao Y, Xue Z, Zhao H, Zhang X (2016) Nanoparticle loading induced morphological transitions and size fractionation of coassemblies from PS-b-PAA with quantum dots. Langmuir 32: 7596-7605
22. Yu Y, Zhang L, Eisenberg A (1998) Morphogenic effect of solvent on crew-cut aggregates of amphiphilic diblock copolymers. Macromolecules 31: 1144-1154
23. Dehghani B, Hosseini MS, Salami-Kalajahi M (2020) Neutral pH monosaccharide receptor based on boronic acid decorated poly (2-hydroxyethyl methacrylate): Spectral methods for determination of glucose-binding and ionization constants.

Microchem J 157: 105112

24. Van Hest JCM, Delnoye DAP, Baars MWPL, Van Genderen MHP, Meijer EW (1995) Polystyrene-dendrimer amphiphilic block copolymers with a generation-dependent aggregation. Science 268: 1592-1595
25. Jung YS, Jung W, Ross CA (2008) Nanofabricated concentric ring structures by templated self-assembly of a diblock copolymer. Nano Lett 8: 2975-2981
26. Dehghani E, Barzgari-Mazgar T, Salami-Kalajahi M, Kahaie-Khosrowshahi A (2020) A pH-controlled approach to fabricate electrolyte/non-electrolyte janus particles with low cytotoxicity as carriers of DOX. Mater Chem Phys 249: 123000
27. Skandalis A, Sentoukas T, Giaouzi D, Kafetzi M, Pispas S (2021) Latest advances on the synthesis of linear ABC-type triblock terpolymers and star-shaped polymers by RAFT polymerization. Polymers 13: 1698
28. Gheitarani B, Golshan M, Safavi-Mirmahalleh S-A, Salami-Kalajahi M, Hosseini MS, Alizadeh AK (2023) Fluorescent polymeric sensors based on N-(rhodamine-6G) lactam-N'-allyl-ethylene-diamine and 7-(allyloxy)-2H-chromen-2-one for Fe^{3+} ion detection. Colloids Surf A: Physicochem Eng Asp 656: 130473
29. Chong YK, Moad G, Rizzardo E, Thang SH (2007) Thiocarbonylthio end group removal from RAFT-synthesized polymers by radical-induced reduction. Macromolecules 40: 4446-4455
30. Zheng H, Bai W, Hu K, Bai R, Pan C (2008) Facile room temperature RAFT polymerization via redox initiation. J Polym Sci Polym Chem 46: 2575-2580
31. Nikravan G, Haddadi-Asl V, Salami-Kalajahi M (2018) Synthesis of dual temperature– and pH-responsive yolk-shell nanoparticles by conventional etching and new deswelling approaches: DOX release behavior. Colloids Surf B-Biointerfaces 165: 1-8
32. Abdollahi E, Abdouss M, Salami-Kalajahi M, Mohammadi A (2016) Molecular recognition ability of molecularly imprinted polymer nano- and micro-particles by reversible addition-fragmentation chain transfer polymerization. Polym Rev 56: 557-583
33. Fallahi-Sambaran M, Salami-Kalajahi M, Dehghani E, Abbasi F (2018) Investigation of different core-shell toward Janus morphologies by variation of surfactant and feeding composition: A study on the kinetics of DOX release. Colloids Surf B-Biointerfaces 170: 578-587
34. Fallahi-Sambaran M, Salami-Kalajahi M, Dehghani E, Abbasi F (2019) Investigating Janus morphology development of poly (acrylic acid)/poly(2-(dimethylamino)ethyl methacrylate) composite particles: An experimental study and mathematical modeling of DOX release. Microchem J 145: 492-500
35. Sharifzadeh E, Salami-Kalajahi M, Hosseini MS, Aghjeh MKR (2017) Synthesis of silica Janus nanoparticles by buoyancy effect-induced desymmetrization process and their placement at the PS/PMMA interface. Colloid Polym Sci 295: 25-36
36. Saito N, Kagari Y, Okubo M (2006) Effect of colloidal stabilizer on the shape of polystyrene/poly (methyl methacrylate) composite particles prepared in aqueous medium by the solvent evaporation method. Langmuir 22: 9397-9402
37. Amirshaqaqi N, Salami-Kalajahi M, Mahdavian M (2014) Corrosion behavior of aluminum/silica/polystyrene nanostructured hybrid flakes. Iran Polym J 23: 699-706
38. Saito N, Nakatsuru R, Kagari Y, Okubo M (2007) Formation of “snowmanlike” polystyrene/poly (methyl methacrylate)/toluene droplets dispersed in an aqueous solution of a nonionic surfactant at thermodynamic equilibrium. Langmuir 23: 11506-11512
39. Torza S, Mason SG (1970) Three-phase interactions in shear and electrical fields. J Colloid Interface Sci 33: 67-83
40. Sakti SP, Amaliya L, Khusnah NF, Masruroh M (2017) Effect of UV radiation duration and molecular weight to hydrophobicity and surface roughness of polystyrene coating on QCM sensor. J Teknol 79: 61-67